Materials Letters 165 (2016) 119–122

Contents lists available at ScienceDirect

Materials Letters

journal homepage: www.elsevier.com/locate/matlet

Microfabricated porous silicon backbone for stable neural interfaces

Tao Sun [a,*], Wei Mong Tsang [a,b], Woo-Tae Park [a,c,**]

[a] Institute of Microelectronics, Agency for Science, Technology and Research (A * STAR), Singapore 117685, Singapore
[b] The Hong Kong Applied Science and Technology Research Institute, Hong Kong Special Administrative Region
[c] Department of Mechanical and Automotive Engineering, Seoul National University of Science and Technology, 139-743 Seoul, South Korea

ARTICLE INFO

Article history:
Received 7 June 2015
Received in revised form
11 November 2015
Accepted 22 November 2015
Available online 23 November 2015

Keywords:
Neural electrode
Microfabrication
Porous Si

ABSTRACT

To fabricate a porous silicon–polymer hybrid neural electrode with the capability of adaptive stiffness, a critical microfabrication process was developed and the porous silicon (PSi) backbone of the neural electrode was prepared for mass production on 8-in. wafers via microelectromechanical systems (MEMS) technologies. Surface characteristics of the microfabricated PSi backbone were determined using scanning electronmicroscopy (SEM), transmission electron microscopy (TEM) and Fourier transform infrared spectrum (FTIR). Moreover, acute cytotoxicity of the PSi backbone was assessed by seeding a mouse fibroblast cell line (L929) on the surface. After 2 days of culture, morphology of cells was observed using a fluorescence microscope, and relative cell viability was also used to quantitatively evaluate the cytotoxicity. Compared to Si samples, relative cell attachment of PSi samples was 192.77 ± 27.19% due to the nano featured surface providing more suitable sites for cell adhesion, indicating that the microfabricated PSi backbone was cytocompatible.

1. Introduction

Neural prostheses can restore the lost body motor functions for paralyzed patients via recording extracelluar potentials from surrounding neurons. Subsequently the neural signals are decoded into intended movements, therefore patients can operate computers or robots with the brain activities [1–3]. However, the longevity of the conventional Si-based neural prostheses cannot meet market requirements mainly due to the long-term neural recording instability. A clinical study for a tetraplegic human with the aim of restoring lost motor functions via a pilot neuromotor prosthesis found abrupt signal loss at most electrodes after 11 months of implantation [4]. The major mechanism of the signal failure is thought to be reduced neuronal cell density, encapsulation of fibrous tissues surrounding the neural electrode to record signals, as well as post-implantation injury as a result of a significant mismatch in mechanical properties between Si (~170 GPa) and cortical tissue (~10 KPa) [5].Therefore, many scientific and technological efforts are devoted to reducing reactive cortical tissue responses by means of designing various neural probe geometries, employing more biocompatible and flexible materials, incorporating drug delivery system into the neural prosthesis, etc. [6–9].

Compared to other approaches to reduce the tissue encapsulation, the neural electrode with adaptive stiffness is attracting ever-growing attention, since it has not only enough strength to penetrate through the dura, but can also significantly reduce the Young's modulus to get closer to the cortical tissue modulus. As porous Si (PSi) has been proposed as a potential electrode material [10], we are proposing a novel strategy to establish stable neural interfaces, and developing a PSi-polymer hybrid neural electrode with a biodegradable PSi backbone which can withstand the insertion force to penetrate into cortical tissue. Due to the degradation of the PSi backbone, the remaining thin insulating polymeric layers (parylene, 5–10 μm) maintains flexibility to minimize post-implantation injury. Hence, this study is the first to report critical microfabrication processes to prepare PSi backbones of the neural electrode on 8-in. wafers, using microelectromechanical systems (MEMS) technologies for mass production. Additionally, the surface characteristics and cytocompatibility of the PSi backbone were investigated as the first step to ensure the long-term safe use of the neural electrode in human body.

2. Materials and methods

8-in. Si wafers (p-type, (100) oriented, 0.002–0.005 Ω cm) used in this study were purchased from Sumco (Sumco Corp. Japan).The microfabrication process of the PSi backbone is illustrated in Fig. 1. After a cleaning using standard piranha solution (a mixture of sulfuric acid and hydrogen peroxide with a ratio of 3:1) for 10 min

* Corresponding author.
** Corresponding author at: Institute of Microelectronics, Agency for Science, Technology and Research (A * STAR), Singapore 117685, Singapore.
E-mail addresses: taosun@hotmail.com.hk (T. Sun), wtpark@seoultech.ac.kr (W.-T. Park).

http://dx.doi.org/10.1016/j.matlet.2015.11.099
0167-577X/

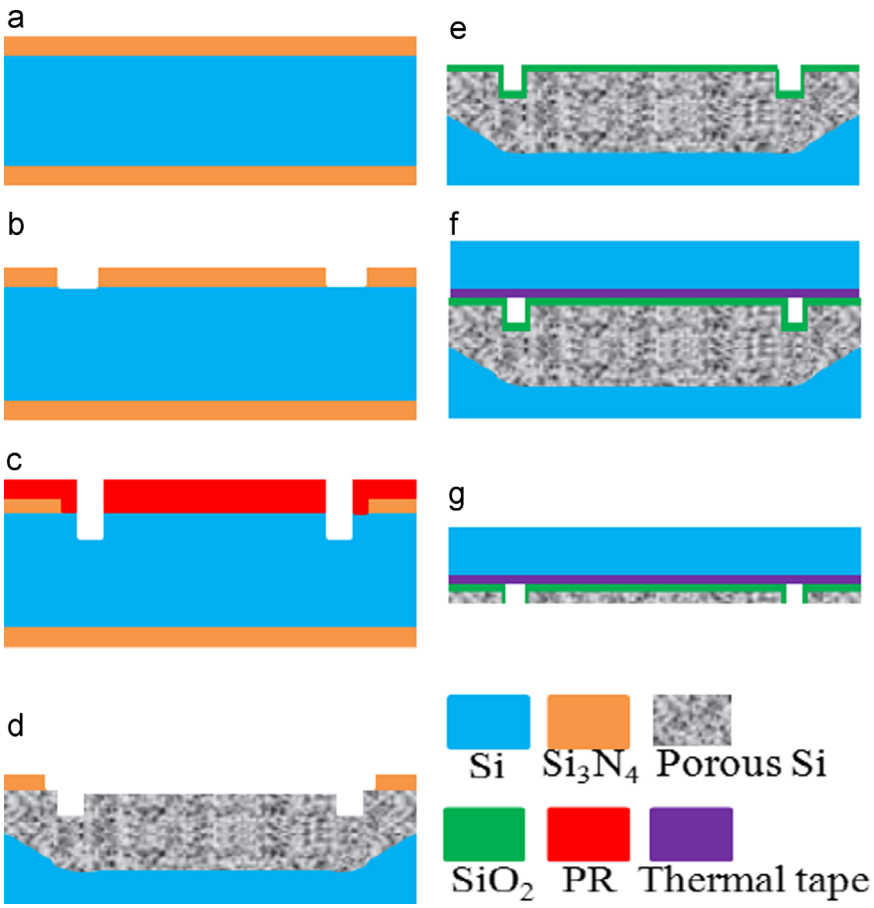

Fig. 1. Microfabrication processes of the PSi backbone: (a) coating LPCVD Si_3N_4 layers on both sides of the wafer; (b) patterning the profile of the probe and area to be anodized; (c) Trench etching by DRIE and PR removal; (d) back-side Si_3N_4 layer removal and anodizing patterned Si wafer; (e) Coating SiO_2 layer; (f) bonding to the handle wafer and back-side grinding; (g) DRIE and thermal release.

and rinse by distilled water, 0.6 μm thick SiN_x layers were deposited on both sides of the Si wafer via low pressure chemical vapor deposition (LPCVD) technology as the hard mask to trench and porisify Si (Fig. 1a). Subsequently, a layer of positive photo resist (PR) was coated and the profile of the neural probe was patterned (Fig. 1b). After a deep reactive ion etching (DRIE) process to form deep trenches (70 μm) into the Si substrate (Fig. 1c), the backside SiN_x layer was etched away through a dry etching method. Prior to etching the front side SiN_x mask, anodization was carried out for the patterned Si to form PSi shanks (Fig. 1d), at a current of 3.5 A, in a 1:1 (v/v) mixture of aqueous hydrofluoric acid (49% HF) and ethanol (99.5%), for 35 min. After the removal of front-side Si_3N_4 mask, a layer of SiO_2 was deposited to prevent PSi backbones from the potential contamination of thermal tape (Fig. 1e). The anodized and patterned wafer was then bonded to a handle wafer via a layer of double-side thermal tape (Fig. 1f). A back-side grinding process was performed to attenuate the thickness of the patterned wafer to 200 μm, followed by exposing PSi layer through a DRIE etch-back process (Fig. 1g). Finally, the PSi backbone was thermally released from a handle wafer.

After the anodization process, the surface morphology of the PSi was examined using scanning electron microscopy (SEM, JSM-6700F, JEOL). The pore size on the surface of PSi was measured using the image analysis tools in ImageJ (National Institutes of Health, USA). The phase composition analysis of the PSi was carried out through transmission electron microscopy (TEM, FEI/Philips Electron Optics, Netherlands). The chemical composition of the surface of the PSi was determined using a Spectrum Spotlight 200 Fourier transform infrared (FTIR) microscope system. Based on ISO 10993–5: 2009, a mouse fibroblast cell line (L929, ATCC, USA) was used to evaluate the cytotoxicity of the PSi backbone [11]. Pure Si backbone with the same dimension as the PSi one

served as the negative control, while latex plates (5 mm × 5 mm) were used as positive control [12]. L929 cells were seeded at 1×10^6 cells/mL onto the surfaces of samples, and relative cell viability of PSi samples was determined by live/dead cytotoxicity assay. After 2 days of culture, live and dead L929 cells were stained in green and red, respectively, and visualized using a fluorescence microscope (Olympus BX61, Olympus Optical Co., Japan). Relative cell attachment of the PSi backbone was calculated by normalizing the number of living cells on its surface with those on Si backbone, while cell viability of Si and PSi backbones at day 2 was obtained by dividing the number of living cells on sample surface into the number of both living and dead cells on its surface. The number of living and dead cells on the surface of the Si and PSi backbones was counted from the fluorescence images. At least 7 areas were randomly chosen for the cell attachment assessment. Results are expressed as means ± standard deviation, and statistical analyses were carried out using a one-way analysis of variance (ANOVA) with Turkey's test of significance between individual groups. $P < 0.05$ is considered statistically significant.

3. Results and discussion

According to the microfabrication process shown in Fig. 1, PSi backbone was successfully developed and released. Fig. 2a shows the optical image of the microfabricated 70 μm-thick PSi backbone with the comb-like structure. The dimension of the backend is

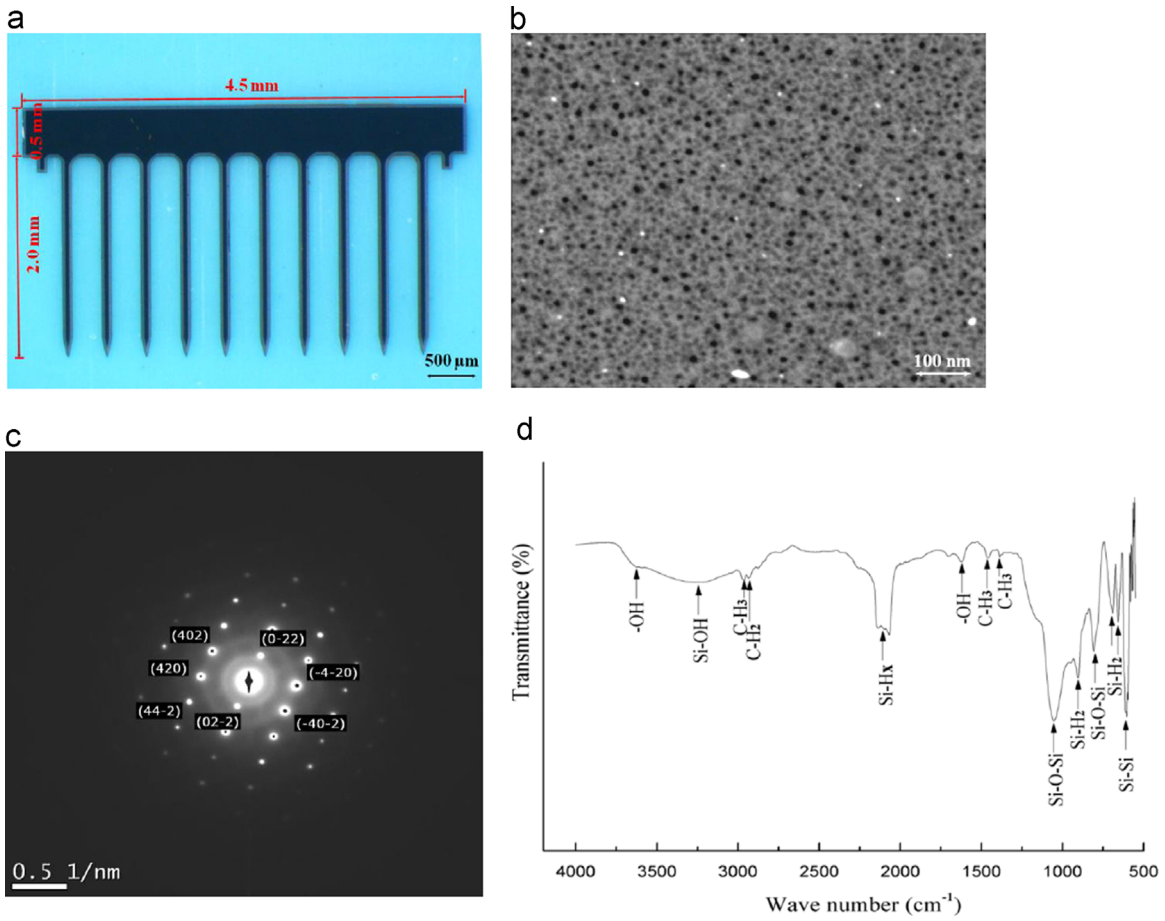

Fig. 2. Surface characterization of the PSi: (a) Optical image of the PSi backbone; (b) surface morphology of the PSi after anodization; (c) SAED pattern of the PSi; (d) FTIR spectra of the PSi surface.

4.5 mm × 0.5 mm. The length and the width of the shanks are 2.0 mm and 100 μm, respectively. The porous structure of the PSi backbone was visualized in Fig. 2b. Irregular pores (11.1 ± 7.6 nm) uniformly distributed on the surface of PSi. Hence, mesoporous Si was formed after the anodization process. The selective area electron diffraction (SAED) pattern of PSi (Fig. 2c) with a [−122] zone axis was labeled and showed the spotty pattern only, revealing that the PSi was well-defined single crystal and the anodization process did not alter the single crystal nature of the bulk material. Fig. 2d displays the FTIR spectrum of the PSi after the anodization process. The band centered at 610 cm^{-1} is due to the stretching vibration of Si–Si bond [13], and Si–H_2 peaks were observed 656, 685 and 910 cm^{-1} [14]. In addition, the bends at 806 and 1056 cm^{-1} were attributed to bending and stretching vibrations of Si–O–Si bond, respectively [15]. More importantly, as the FTIR characteristic peak of PSi, the broad band in the range 2060–2150 cm^{-1} was present in the FTIR spectrum owing to Si–H_x (x=1, 2, and 3) stretching modes [16], reconfirming the formation of the PSi. As the mixture of aqueous hydrofluoric acid and ethanol was used as the electrolyte to porosify Si, CH_3 and CH_2 functional groups arising from ethanol were identified from the FTIR spectrum, and O–H stretching vibration of absorbed H_2O resulted in the band at 3600 cm^{-1}.

After 2 days of culture, morphology of L929 cells seeded on latex, Si and PSi backbones was shown in Fig. 3a, b and c, respectively. Because of the cytotoxicity of latex, few cells attached on its surface and no living cells were observed under the fluorescence microscope (Fig. 3a). On Si backbone, most L929 cells appeared flattened, with a wide-spread and round cytoplasm, while a few cells were elongated and showed a typical spindle-like morphology (Fig. 3b). Cells grown on PSi backbone seemed more aggregated and more round, but displayed a smaller size (Fig. 3c). Cell viability of Si and PSi backbones was 93.83 ± 3.98% and 95.27 ± 1.41% at day 2, respectively ($P > 0.05$). Furthermore, more living cells were observed on PSi backbone ($P < 0.05$) and this phenomenon can be ascribed to the nano featured PSi surface, which provided more sites for cell adhesion. It was reported that extracellular matrix (ECM) surrounding the cells, surface topography of biomaterials, physical and chemical interactions at cell-biomaterials interface play critical roles in cell attachment [17]. Collart-Dutilleul et al. suggested that PSi with pore size of ~36 nm was able to mimic ECM environment properties to promote cell attachment [18]. Filopodia are needle-shaped, actin-driven cell protrusions (roughly 2–3 μm length and 200–300 nm width), and form focal adhesions with substrates, linking it to the cell surface. Besides, they have functions of sensing surrounding environment, guiding cell migration towards sites of interest, and acting as sites for signal transduction. PSi was demonstrated to enhance the formation of lateral actin microfilaments protruding from cell body and from lamellipodia area, and had positive effects on filopodia growth [18]. As a consequence, PSi was believed to provide more anchorage points for cell attachment. Although it was believed that PSi bulk material or particles were promising biomaterials for tissue engineering or drug release, the microfabricated PSi devices have been rarely reported and their biocompatibility has not been extensively studied. In this study, PSi backbone was not only successfully developed by the microfabrication process, but also cytocompatible on the basis of *in vitro* results. More importantly, the microfabrication process reported in the study consists of standard MEMS technologies, and therefore is suitable for mass production in industry.

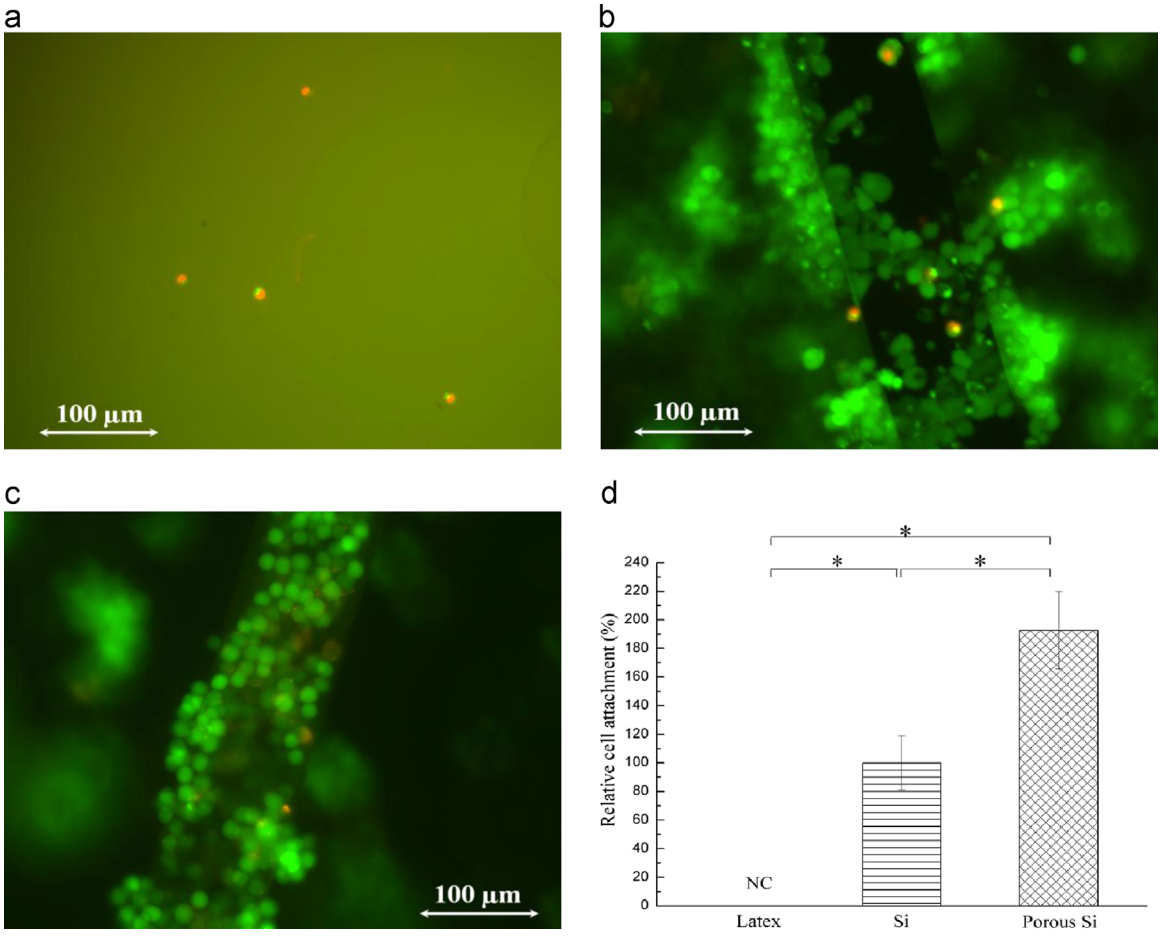

Fig. 3. At day 2, morphology of L929 cells seeded on (a) Si and (b) PSi surfaces, and (c) relative cell attachment of L929 on latex, Si and PSi surfaces. NC: no living cells were observed. The statistical significance is indicated by $^{*}(P < 0.05)$.

4. Conclusions

The microfabrication process of the PSi backbone was successfully developed for the novel neural electrode via standard MEMS technologies, and suitable for mass production. PSi with average pore size of 11.1 ± 7.6 nm was formed after the anodization process. Due to its nano featured surface facilitating cell adhesion, relative cell attachment of PSi samples was $192.77 \pm 27.19\%$ in comparison with that of Si samples after 2 days of cell culture. Moreover, there was no significant difference in cell viability between Si and PSi backbones at day 2 ($P > 0.05$), revealing that the PSi backbone did not exhibit acute cytotoxicity.

Acknowledgments

This work was supported by the Science and Engineering Research Council of Agency for Science, Technology and Research (A*STAR) under Grant 1021710159, and by the Basic Science Research Program through the National Research Foundation of Korea (NRF) funded by the Ministry of Science, ICT and Future Planning (NRF-2013R1A1A1012616).

References

[1] J.K. Chapin, Nature 442 (2006) 452–455.
[2] Nicolelis MAL, Nature 409 (2001) 403–407.
[3] T. Sun, W.-T. Park, M.Y. Chen, J.Z. An, R.F. Xue, K.L. Tan, M. Je, IEEE Trans. Biomed. Eng. 59 (2012) 390–399.
[4] L.R. Hochberg, M.D. Serruya, G.M. Friehs, J.A. Mukand, M. Saleh, A.H. Caplan, A. Branner, D. Chen, R.D. Penn, J.P. Donoghue, Nature 442 (2006) 164–171.
[5] V.S. Polikov, P.A. Tresco, W.M.J. Reichert, Neurosci. Methods 148 (2005) 1–18.
[6] J.P. Seymour, D.R. Kipke, Biomaterials 28 (2007) 3594–3607.
[7] A. Blau, A. Murr, S. Wolff, E. Sernagor, P. Medini, G. Iurilli, C. Ziegler, F. Benfenati, Biomaterials 32 (2011) 1778–1786.
[8] S.P. Khan, G.G. Auner, O. Palyvoda, G.M. Newaz, Mater. Lett. 65 (2011) 876–879.
[9] M.R. Abidian, D.C. Martin, Adv. Funct. Mater. 19 (2009) 573–585.
[10] F. Johansson, L. Wallman, N. Danielsen, J. Schouenborg, M. Kanje, Acta Biomater. 5 (2009) 2230–2237.
[11] Y.B. Wang, Y.F. Zheng, Mater. Lett. 63 (2009) 1293–1295.
[12] T. Sun, W.-T. Park, W.M. Tsang, T.B. Yee, M. Je, Nanosci. Nanotechnol. Lett. 5 (2013) 916–920.
[13] T.F. Young, C.P. Chen, J.F. Liou, Y.L. Yang, T.C. Chang, J. Porous Mater. 7 (2000) 339–343.
[14] M.R. Nangrejo, M.J. Edirisinghe, J. Porous Mat. 9 (2002) 131–140.
[15] G. Shi, G. Xu, G. Han, Matter Lett. 61 (2007) 463–465.
[16] Z.C. Feng, A.T.S. Wee, K.L. Tan, J. Phys. D: Appl. Phys. 27 (1994) 1968.
[17] A.L. Berrier, K.M. Yamada, J. Cell. Physiol. 213 (2013) 565–573.
[18] P. Collart-Dutilleul, I. Panayotov, E. Secret, F. Cunin, C. Gergely, F. Cuisinier, M. Martin, Nanoscale Res. Lett. 9 (2014) 564.